ARTICLES

Structure and hydration of membranes embedded with voltage-sensing domains

Dmitriy Krepkiy[1]*, Mihaela Mihailescu[2,5]*, J. Alfredo Freites[2,3], Eric V. Schow[4], David L. Worcester[2,5,6], Klaus Gawrisch[7], Douglas J. Tobias[3], Stephen H. White[2,5] & Kenton J. Swartz[1]

Despite the growing number of atomic-resolution membrane protein structures, direct structural information about proteins in their native membrane environment is scarce. This problem is particularly relevant in the case of the highly charged S1–S4 voltage-sensing domains responsible for nerve impulses, where interactions with the lipid bilayer are critical for the function of voltage-activated ion channels. Here we use neutron diffraction, solid-state nuclear magnetic resonance (NMR) spectroscopy and molecular dynamics simulations to investigate the structure and hydration of bilayer membranes containing S1–S4 voltage-sensing domains. Our results show that voltage sensors adopt transmembrane orientations and cause a modest reshaping of the surrounding lipid bilayer, and that water molecules intimately interact with the protein within the membrane. These structural findings indicate that voltage sensors have evolved to interact with the lipid membrane while keeping energetic and structural perturbations to a minimum, and that water penetrates the membrane, to hydrate charged residues and shape the transmembrane electric field.

Membrane-embedded S1–S4 voltage-sensing domains are used by membrane proteins to sense and react to changes in membrane voltage (Fig. 1a). In the voltage-activated potassium (K_v), sodium and calcium channels, these domains drive opening and closing of an associated ion-conducting pore domain (Fig. 1a) to generate electrical signals[1]. In the *Ciona intestinalis* voltage-sensitive phosphatase, an S1–S4 domain controls the hydrolysis of phospholipids by an associated phosphatase[2], and in voltage-activated proton channels, the S1–S4 domain contains the permeation pathway for protons[3]. X-ray structures of S1–S4 domains show that the protein domain comprises four transmembrane α-helices (Fig. 1a) and that its structure is well conserved in organisms ranging from archaebacteria to mammals[1,4,5].

A fundamental feature of S1–S4 domains is that they contain basic and acidic residues that enable the protein to change conformation in response to rapid fluctuations in membrane voltage[1,6,7]. In these voltage sensors, interactions with the surrounding lipid membrane have crucial roles. The S3b–S4 paddle motif within S1–S4 domains, for example, moves at the protein–lipid interface[5,8–13], and alterations in the composition of the lipid membrane alter voltage-sensor activation[14–17]. The polar nature of voltage sensors and their intimate interactions with the bilayer raise the possibility that these domains perturb the structure of the surrounding lipid bilayer. In addition, although spectroscopic and functional studies suggest that the electric field is focused across voltage sensors[18–21], the structural basis for focusing is unclear. It is not known whether deformations of the membrane contribute to focusing the electric field or whether the shape and chemistry of the protein are mainly responsible. Crevices observed in X-ray structures of S1–S4 domains would be expected to reshape the electric field, but only if they persist and are filled with water when the domain is embedded in a lipid membrane. Although water penetration of the membrane has been inferred from accessibility studies[9,13,19,22–26] and simulations[12,27–29], hydration of voltage sensors has not been measured.

Structure and hydration of membranes containing voltage sensors

To address these fundamental issues, we developed a homogeneous preparation of voltage-sensing domains incorporated into lipid membranes for use with neutron diffraction[30–33]. The neutron scattering length gives the relative amplitude of the de Broglie wave scattered from a nucleus and is analogous to the X-ray scattering length of an electron. We focused our efforts on the S1–S4 domain of K_vAP, an archaebacterial channel from *Aeropyrum pernix* that can be robustly expressed, stably purified and reconstituted into lipid membranes[4,9,10,13,34]. After expression and purification of the S1–S4 domain of K_vAP (Methods), circular dichroism spectroscopy reveals that the domain has high α-helical content in detergent micelles or reconstituted into liposomes (Fig. 1b), consistent with the X-ray structure of the domain[4] and electron paramagnetic resonance studies[9,13,34]. To investigate the topology of the S1–S4 domain in liposomes, we measured the fluorescence of the single Trp 70 residue near the middle of the S2 helix. The emission spectrum of Trp 70 is shifted towards shorter wavelengths relative to that of free Trp in aqueous solution (Fig. 1c), indicating that Trp 70 resides in a non-polar environment[35]. Moreover, its fluorescence is efficiently quenched by bromine atoms covalently bound to lipid hydrocarbon tails[36] but not by the aqueous quencher acrylamide (Fig. 1c–e), consistent with the S2 helix having a transmembrane topology (see below).

To determine the profile structure of bilayers containing S1–S4 domains, we produced oriented lipid multilayers by deposition of proteoliposomes or neat liposomes on glass substrates. When these multilayers were hydrated (86 or 93% relative humidity) and mounted in a cold neutron beam[37], we observed strong lamellar

[1]Molecular Physiology and Biophysics Section, Porter Neuroscience Research Center, National Institute of Neurological Disorders and Stroke, National Institutes of Health, Bethesda, Maryland 20892, USA. [2]Department of Physiology and Biophysics, and Center for Biomembrane Systems, [3]Department of Chemistry and Institute for Surface and Interface Science, [4]Department of Physics and Astronomy and Institute for Genomics and Bioinformatics, University of California, Irvine, California 92697, USA. [5]NIST Center for Neutron Research, National Institute of Standards and Technology, Gaithersburg, Maryland 20899, USA. [6]Biology Division, University of Missouri, Columbia, Missouri 65211, USA. [7]Laboratory of Membrane Biochemistry and Biophysics, National Institute on Alcohol Abuse and Alcoholism, National Institutes of Health, Bethesda, Maryland 20892, USA.
*These authors contributed equally to this work.

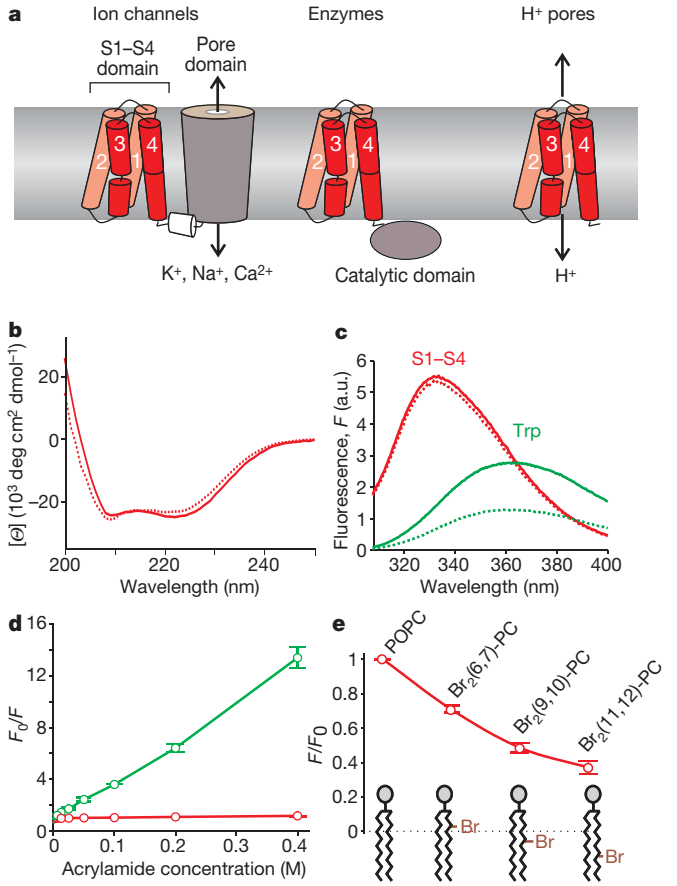

Figure 1 | S1–S4 voltage-sensing domains and their biophysical properties in lipid bilayers. **a**, Representation of membrane proteins containing S1–S4 voltage-sensing domains (red), embedded in the lipid bilayer (light grey). **b**, Circular dichroism spectra of the S1–S4 voltage-sensing domain of K_vAP in octyl glucoside micelles (dotted red line) and reconstituted into 1-palmitoyl-2-oleoyl-*sn*-glycero-3-phosphocholine (POPC) and 1-palmitoyl-2-oleoyl-*sn*-glycero-3-[phospho-*rac*-(1-glycerol)] (POPG) proteoliposomes at a protein/lipid molar ratio of 1:130 (solid red line). The spectra indicate high (~85%) helical content (Methods). [Θ], mean residue ellipticity. **c**, Fluorescence emission spectra of Trp 70 within the S1–S4 voltage-sensing domain after reconstitution in POPC–POPG (protein/lipid molar ratio of 1:100) in the absence (solid red line) and presence (dotted red line) of 50 mM aqueous acrylamide. Also shown are the emission spectra of free Trp (25 μM) mixed with POPC–POPG liposomes of identical lipid concentration in the absence (solid green line) and presence (dotted green line) of 50 mM aqueous acrylamide. a.u., arbitrary units. **d**, Stern–Volmer plots for acrylamide quenching of fluorescence emission of Trp 70 within the S1–S4 voltage-sensing domain (red) and of free Trp (green). Error bars, s.e.m. ($n = 3$). The Stern–Volmer constant for quenching was $0.4 \pm 0.02\ M^{-1}$ for Trp 70 and $26.2 \pm 0.2\ M^{-1}$ for free Trp. F_0, fluorescence in absence of a quencher. **e**, Quenching of fluorescence emission of Trp 70 within the S1–S4 voltage-sensing domain by bromine atoms attached at different positions along the lipid hydrocarbon tail. The protein was reconstituted into the 1:1 mixture of POPG and either POPC or one of three dibrominated phosphatidylcholines (PCs), Br_2(6,7)-PC, Br_2(9,10)-PC or Br_2(11,12)-PC (Methods). Error bars, s.e.m. ($n = 3$).

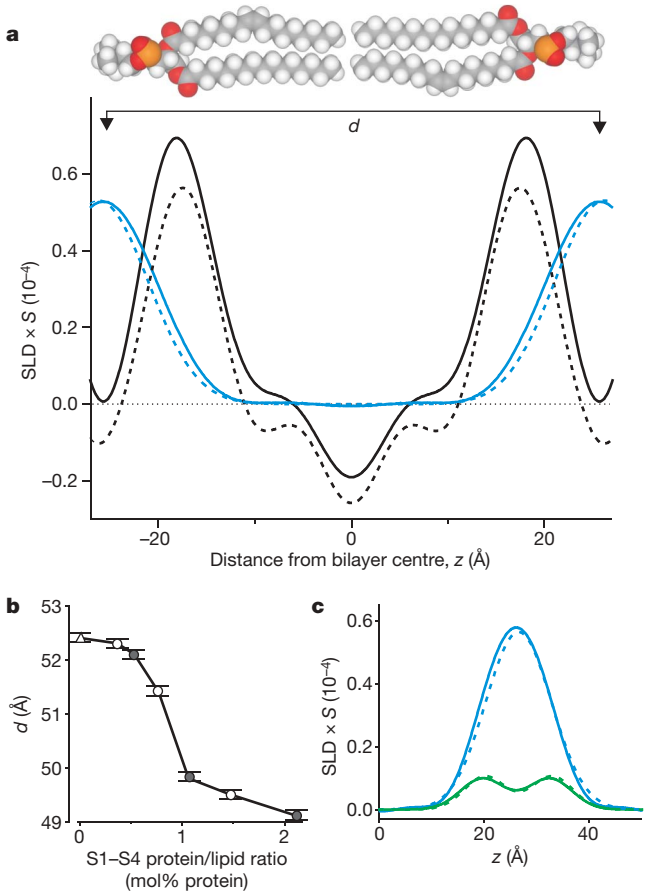

Figure 2 | Scattering-length density profiles for bilayers containing S1–S4 voltage-sensing domains. **a**, Scattering-length density profiles, on an absolute scale[32], of the S1–S4 voltage-sensing domain in lipid bilayers (black solid line) and the water distribution (blue solid line). The protein/lipid molar ratio is 1:130 (0.77 mol%) and relative humidity is 86%. Profiles for lipid in the absence of protein (dashed lines) are shown for comparison. The density profile amplitudes are presented in units of scattering length per unit length, corresponding to the scattering-length density (SLD) of a unit cell (POPC/POPG/protein ratio, 0.4962:0.4962:0.0076; plus 8.5 water molecules) multiplied by the area per lipid (S; Methods). The x axis shows the distance from the bilayer centre (z), with the origin positioned in the middle of the bilayer. A space-filling model of POPC is shown above the plot (hydrogen, white; carbon, grey; oxygen, red; phosphorous, yellow). **b**, Effect of S1–S4 voltage sensing domains on the bilayer thickness at different protein/lipid ratios. The triangle marks the value of d for neat-lipid bilayers. Open circles are for voltage-sensing domains with His tag removed (Methods) and filled circles are for the His-tagged protein. Error bars represent 1 s.d., obtained from least-squares fitting of angular positions of the Bragg peaks. **c**, Distribution of deuterium atoms in head-group-labelled phosphocholine (-C^2H_2-C^2H_2-; D4 lipid) in bilayers containing S1–S4 domains (solid green line) and comparison with the distribution of water (solid blue line). Dashed lines show the distributions of D4 lipid and water in the absence of the protein. The protein/lipid ratio is as in **a** and 25-mol% D4-POPC is used in the mixture of POPC and POPG. The relative humidity is 93%.

diffraction patterns with Bragg spacing d (Supplementary Fig. 1a, b). One-dimensional, absolute-scale, scattering-length density profiles along the normal of the lipid bilayer plane were then computed from the observed structure factors (Fig. 2a). The constructed neutron scattering-length density profiles for neat-lipid bilayers show the distribution of lipid (black dashed line), with positive densities for the head-group region, a trough for the hydrocarbon tails and negative densities near the terminal methyl groups (Fig. 2a). The scattering lengths for most of the relevant nuclear species (carbon, nitrogen, oxygen and phosphorous) have similarly positive values; a notable exception is hydrogen, which has a negative scattering length. The average scattering-length density of the bilayer hydrocarbon core is close to zero because the scattering length of carbon is positive and that of hydrogen is negative. The head-group peaks appear closer together than they would in an equivalent X-ray experiment[33] because X-rays scatter most strongly from head-group phosphates, whereas neutrons scatter most strongly from the carbonyl groups owing to their relative lack of hydrogen atoms.

The overall scattering-length density of the bilayer increases in the presence of the protein (Fig. 2a, solid black line), consistent with the S1–S4 domain having a transmembrane topology (see below).

Comparison of the lipid bilayer profiles with and without S1–S4 domains reveals how the structure of the bilayer is influenced by the protein (Fig. 2a). Although the S1–S4 domain does not radically alter the structure of the lipid bilayer, examination of the profiles shows that the voltage sensors produce a detectable thinning of the bilayer, as revealed by a decrease in d (Fig. 2b). The thickness decrease depends on the concentration of the protein in the membrane, with a maximal decrease of about 3 Å at protein/lipid molar ratios greater than 1:100 (Fig. 2b). These results indicate that lipid molecules in the membrane maintain a bilayer-like arrangement around voltage sensors, consistent with the lipids resolved in the recent crystal structure of the $K_v1.2/2.1$ paddle chimaera[5].

Next we performed experiments to determine the distribution of water and to quantify the number of water molecules per lipid by using contrast variation between water (^1H_2O) and deuterium oxide (^2H_2O) and by comparing with lipids containing four deuterium atoms in the head-group region (D4 lipids; Fig. 2c; Methods). This approach takes advantage of the fact that deuterated nuclei have a positive scattering length whereas that of hydrogen is negative; selective substitution of deuterium for hydrogen therefore allows the deuterium atoms to be easily detected against the low scattering-length density of the hydrocarbon core. Although the water distributions show that thinning of the bilayer brings water on the two sides of the bilayer closer together (Fig. 2a, blue lines), we could not detect a change in the shape of the water distribution or the total water content. At 86% relative humidity, the unit cell of the membrane contains 8.1 ± 0.7 water molecules per lipid for neat-lipid bilayers, compared with 8.5 ± 0.5 in the presence of 0.77-mol% protein. At 93% relative humidity, water content was 10.6 ± 0.2 molecules per lipid in the absence of 0.77-mol% protein and 11.0 ± 0.2 molecules per lipid in its presence (Supplementary Fig. 2).

Distributions of S1–S4 voltage-sensing domains and water across membranes

To investigate the membrane topology and hydration of S1–S4 domains directly, we determined the protein distribution using contrast variation between protonated and deuterated S1–S4 domains. The S1–S4 domain of K_vAP was uniformly deuterated to 74% (Fig. 3a) and multilayers were formed with either protonated or deuterated protein at the same protein/lipid ratio and lipid composition. The two types of sample display similar diffraction patterns, with the same number of observed diffraction orders and repeat spacing (Supplementary Fig. 3). Subtraction of scaled profiles to obtain the protein density distribution reveals the distribution of the protein across the bilayer (Fig. 3b, red line). Maxima in the density distribution are observed in the head-group region of the bilayer and minima are observed in the inter-bilayer space. This finding firmly establishes that S1–S4 domains adopt a transmembrane topology when embedded in a lipid membrane, with the four helices oriented roughly normal to the membrane plane. It is not surprising to find a significant protein density in the inter-bilayer space, given that the dimensions of the S1–S4 helices[4,5] are similar to the thickness of the bilayer (and that the helices may protrude somewhat outside the membrane).

Having determined the distribution of protein in the bilayer (Fig. 3b, red), we then compared it to that of water (Fig. 3b, blue) to ascertain whether S1–S4 domains are hydrated. Strikingly, the two distributions have an extensive overlap within the confines of the lipid membrane, in particular for the outer halves of the bilayer. Because the voltage sensor does not detectably alter water content or the shape of the water distribution, the hydration detected in these neutron diffraction experiments is mainly from water that is already present in the bilayer. The voltage sensors may bring additional water molecules into the bilayer, but it is unlikely that we would have yet detected them in the experiments. For example, molecular dynamics simulations predict that 45–47 water molecules intimately associate with each voltage sensor (see below); such association would not

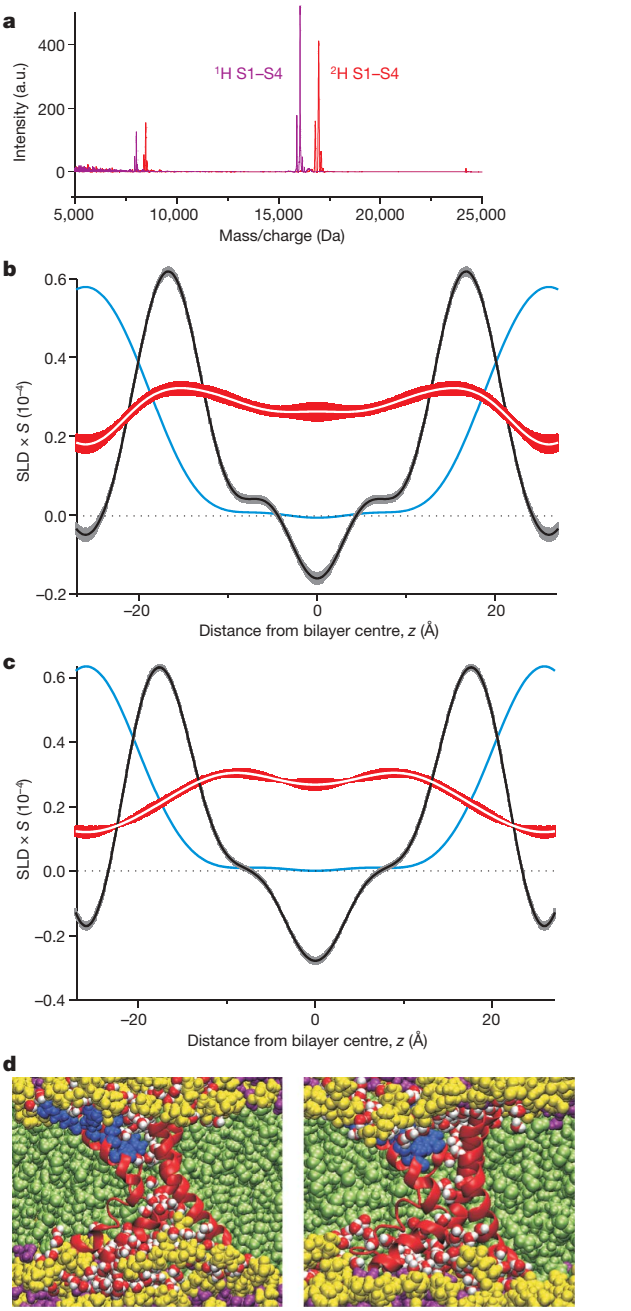

Figure 3 | Deuteration of S1–S4 voltage-sensing domains and distribution of the protein in lipid membranes. **a**, Matrix-assisted laser desorption/ionization (MALDI) mass spectra of the protonated S1–S4 domain of K_vAP (^{1}H S1–S4, purple) and the uniformly deuterated S1–S4 domain (^{2}H S1–S4, red). The difference in mass indicates that the protein is deuterated to 74%. **b**, Trans-bilayer distribution of the S1–S4 domain (white line surrounded by a broad red band) obtained in neutron diffraction experiments from the profile difference between deuterated and protonated S1–S4 domains. Profiles are shown on an absolute (per lipid) scale. Water distribution is shown in blue and lipid as a black line surrounded by a grey band. The broad bands represent estimates of experimental uncertainty computed using the methods of ref. 33. The protein/lipid ratio is 1:130 (0.77 mol%) and the relative humidity is 93%. **c**, Neutron scattering-length density profiles for the simulation system with 11 water molecules per lipid. Trans-bilayer distribution of the S1–S4 domain is shown as a white line surrounded by a broad red band (estimated experimental uncertainty), water is shown in blue and lipid is shown in black. **d**, Snapshots of the region in the vicinity of one of the two voltage-sensing domains from the molecular dynamics simulation of a stack of two bilayers with 11 water molecules per lipid (left) and excess water (right). Water molecules within 6 Å of protein are shown as red–white spheres and all other water molecules are coloured purple. Phosphocholine head groups are coloured yellow and the acyl chains are coloured light green. The ribbon diagram of the S1–S4 domain is coloured red with the outer four Arg residues in S4 shown as blue CPK models.

detectably alter the shape of the water distribution determined in neutron diffraction experiments because these molecules constitute less than 4% of all water molecules in the system for each voltage sensor (at 0.77-mol% protein and 93% humidity, the protein/lipid/water ratio is 1:130:1,430).

Predicted distributions of water, lipid and protein with varying hydration

To explore whether the distributions of water, lipid and protein observed in neutron diffraction experiments are compatible with those predicted from molecular dynamics simulations, we calculated neutron diffraction structure factors from molecular dynamics simulation trajectories for the S1–S4 domain of K_vAP embedded in a lipid bilayer in a transmembrane orientation (Methods). The resulting Bragg spacing is in excellent agreement with the experimental results, and the overall bilayer scattering-length density profile and water distributions, determined by applying the same procedures as in the reduction of the experimental data, are in good agreement with the experimental results (Fig. 3c). Simulation and experiment show comparable overall protein density distributions in the membrane interior, as well as overlap between the distributions of protein and water, suggesting a similar disposition of protein and water in the lipid bilayer. Compared with that used for simulations, the protein studied experimentally contains 18 additional residues on the amino terminus (Methods), precluding a quantitative comparison of the experimental and simulated protein profiles. On the basis of the location of the corresponding segment in the structure of the $K_v1.2/2.1$ paddle chimaera[5], the excess scattering-length density in the experimental data relative to the simulation near the membrane–water interface ($|z| > 10$ Å) can reasonably be attributed to the 18-residue amphipathic segment absent in the simulation.

To explore whether hydration of the preparation influences these distributions, we compared a simulation with 11 water molecules per lipid (corresponding to 93% relative humidity) with a previously reported simulation in a lipid bilayer in excess water[27] (Fig. 3d), finding that the scattering-length density profiles observed in the two cases are similar (Supplementary Fig. 4). The structure of the S1–S4 domain was also relatively insensitive to hydration level (Supplementary Fig. 5), and in each case a similar number of water molecules (45–47 at 11 water molecules per lipid and 48–49 in excess water) are intimately associated with the protein domain within the hydrophobic core of the bilayer (Supplementary Fig. 6). In addition, solvation of crucial S4 Arg residues by both water and phosphate head groups is similarly observed at varying hydration levels (Supplementary Fig. 7). Together these observations suggest that the extent to which hydration of the preparation influences the structure of lipid membranes containing voltage sensors is minor, and would not be discernible in the neutron scattering profiles at the protein concentrations studied.

Interaction between water and S1–S4 voltage-sensing domains

Although the neutron diffraction experiments indicate that the distribution of water and protein in the bilayer overlap, they do not directly address the question of whether water is intimately associated with voltage sensors (Fig. 4a). To explore this possibility, we used solid-state NMR spectroscopy to measure magnetization transfer from water to lipid by means of intermolecular ^{1}H dipole–dipole interactions in the presence of the voltage sensor. Well-resolved lipid resonances (Fig. 4b, black spectra) were observed when the sample was rapidly spun (10 kHz) at an angle of 54.7° (the magic angle) to the magnetic field, a procedure that averages out anisotropic dipolar interactions that broaden resonance lines.

We performed saturation-transfer difference experiments[38,39] by comparing lipid spectra before (Fig. 4b, black spectra) and after (Fig. 4b, blue spectra) applying saturating radio-frequency pulses at the ^1H_2O resonance frequency (chemical shift, 4.79 p.p.m.). Magnetization transfer to lipid would cause a decrease in the intensity of

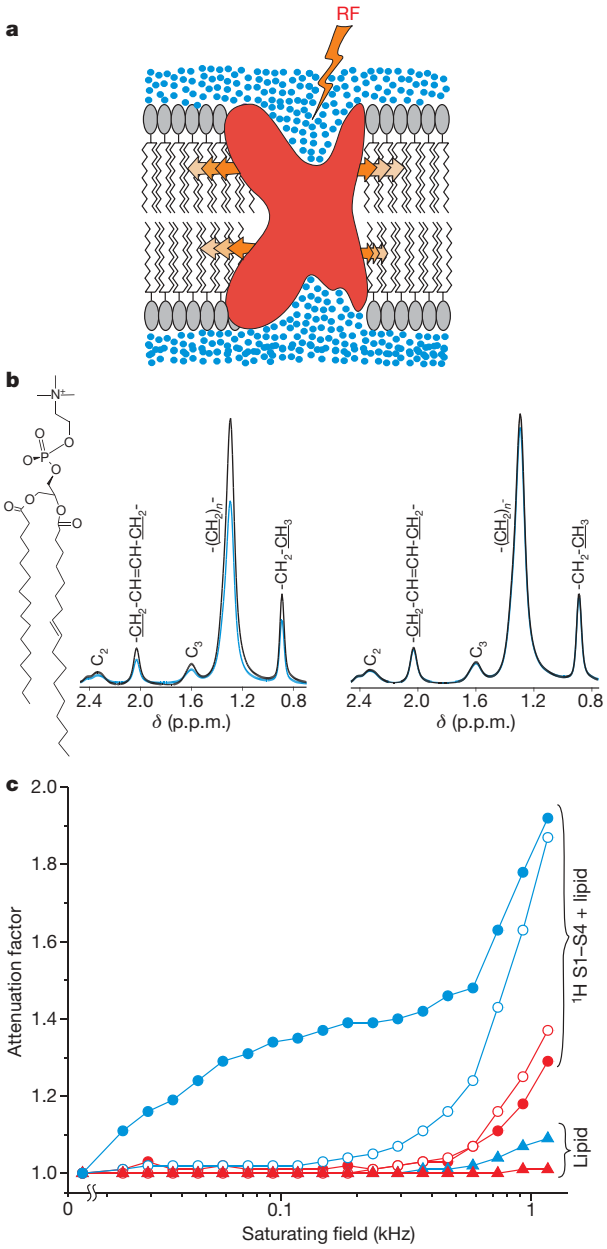

Figure 4 | Interaction of water and S1–S4 voltage-sensing domains within lipid membranes. **a**, Schematic representation of crevices in S1–S4 voltage-sensing domains (red) filled with water (blue) and an experiment in which selective, saturating radio-frequency (RF) pulses were applied at the water resonance (4.79 p.p.m.). Magnetization transfer (arrows) from water through protein to the surrounding lipid results in the attenuation of the lipid ^{1}H NMR signals. **b**, Aliphatic region of magic-angle-spinning ^{1}H NMR spectra of a lipid sample containing S1–S4 voltage-sensing domains in the presence of ^1H_2O (left-hand spectrum) or ^2H_2O (right-hand spectrum). Lipid resonances for both POPC and POPG (present in a 1:1 mix) are indicated on the spectra, with peaks corresponding to underlined ^{1}H atoms. Attenuation of the methylene resonance (1.3 p.p.m.) is observed (blue traces) when saturating radio-frequency pulses (field strength, 232 Hz) are applied at 4.79 p.p.m. to a sample containing ^1H_2O (left), but not to one containing ^2H_2O (right). Field strength is reported in frequency units as $(\gamma/2\pi)B_1$, where γ is the proton gyromagnetic ratio and B_1 is the magnetic component of the radio-frequency pulse. Attenuation is defined as signal intensity recorded without saturation divided by signal intensity recorded with saturation. δ, chemical shift. The structure of POPC is shown on the left. **c**, Attenuation factors plotted as a function of radio-frequency field strength. The carrier radio frequency was set at either the water resonance (4.79 p.p.m., blue) or in the protein amide region (8.5 p.p.m., red). Circles show data for S1–S4 domains in lipid bilayers where the protein/lipid ratio is 1:100. Triangles show data for samples containing lipid alone. Samples containing ^1H_2O are indicated by filled symbols, whereas those containing ^2H_2O are indicated by open symbols.

lipid resonances, which can be quantified as an attenuation factor for different saturating field strengths (Fig. 4c). Control experiments in which neat-lipid membranes were studied show that magnetization transfer from ^1H_2O to lipid is inefficient when radio-frequency pulses are applied to ^1H_2O (Fig. 4c, blue triangles). In the presence of the protein, magnetization transfer is similar in ^1H_2O and ^2H_2O when radio frequency pulses are applied directly to the protein amide resonance frequency (8.5 p.p.m.; Fig. 4c, red filled (^1H_2O) and open (^2H_2O) circles). In contrast, magnetization transfer from water to lipid is very efficient in membranes containing S1–S4 voltage-sensing domains in the presence of ^1H_2O (Fig. 4c, blue filled circles). Much weaker transfer is observed when ^1H_2O is replaced with ^2H_2O (Fig. 4c, blue open circles), demonstrating that most of the attenuation results from magnetization transfer starting from ^1H_2O rather than from resonances of aliphatic hydrogen atoms of the protein that overlap with the water resonances at 4.79 p.p.m. (The attenuation observed in ^2H_2O at a saturating field of >200 Hz probably originate from aliphatic hydrogen atoms.) When considered together with the overlap in water and protein distributions observed in neutron diffraction experiments (Fig. 3b), these NMR results indicate that water intimately associates with the protein within the bilayer.

Discussion

The objective of the present study was to investigate the structure and hydration of lipid membranes containing S1–S4 voltage-sensing domains. Previously, only computational approaches have been used to explore how different types of membrane protein influence the structure of the bilayer[12,27–29,40,41]. We adapted neutron diffraction techniques to determine how voltage sensors influence membrane structure; these protein domains are highly polar and exhibit important interactions with the lipid membrane, making them a particularly interesting test case. We succeeded in reconstructing the bilayer profile in the presence of the S1–S4 domain of K_vAP, which shows that the structure of the lipid bilayer remains largely intact around the protein. The most notable change is that the protein causes a thinning of the bilayer by about 3 Å. Neutron diffraction measurements reflect changes in the structure of the bilayer, averaged over the entire membrane plane. Molecular dynamics simulations, yielding a value of the Bragg spacing consistent with the diffraction experiments, predict that the distortion of the lipid bilayer by the protein is restricted to the lipids immediately surrounding the voltage sensors (Fig. 5a; Supplementary Fig. 8). Taken together, the modest membrane-averaged thinning and local adaptation of the lipid bilayer to the presence of the voltage sensor suggest that the protein has evolved to interact with lipid molecules while minimizing the energetic and structural perturbations of the bilayer.

Our neutron diffraction, solid-state NMR and simulation results indicate that S1–S4 voltage-sensing domains are hydrated in the bilayer and that water interacts intimately with the protein. The observed hydration can explain the accessibility of water-soluble reagents to residues in S1–S4[9,13,19,22–26] and suggests that the crevices seen in X-ray structures[4,5], which house the Arg residues that carry gating charge[6,7], actually contain water when the protein is embedded in a lipid membrane, as illustrated in Fig. 3d. Hydration of these critical residues will raise the local dielectric constant within the bilayer, ensuring that the Arg residues remain charged and thereby move in response to changes in membrane voltage. Consideration of the observed average water distributions in the presence of S1–S4 domains indicates that the membrane electric field decreases over a distance of no more than about 25 Å, which is the hydrophobic thickness of the bilayer in the presence of the voltage-sensing domain. The water-filled crevices in the structure of the S1–S4 domain would be expected to focus the electric field further, in agreement with our simulations showing that the transmembrane potential is contoured by the structure of the protein and decreases over a distance of about 20 Å (Fig. 5b). These simulations do show significant distortions of the lipid bilayer in the local vicinity of the protein (Fig. 5a), but these do not have pronounced effects on the transmembrane voltage.

Although the effects of S1–S4 voltage-sensing domains on the physical thickness of the bilayer are not large, the bilayer thinning we observe indicates that the protein and bilayer do interact, thereby providing a basis for understanding how lipid modification can influence voltage-sensor function[14–17]. For example, on the basis of theoretical considerations and studies of gramicidin channels[42–44], the thinning we observed would be expected to have profound effects on the mechanical properties of channels containing S1–S4 domains and may help to explain the sensitivity of voltage-activated ion channels to alterations in the mechanical properties of the lipid bilayer[41,45–47].

The hydration and reshaping of the lipid membrane that we observe for voltage sensors will probably be relevant for other classes of membrane protein. For example, the presence of binding sites for water-soluble ligands deep within G-protein-coupled receptors[48] and transporters[49] implies that these proteins are hydrated within the membrane. In the case of intramembrane enzymes, such as the rhomboid protease[50], hydrolysis of the peptide bond requires the presence of water molecules in an active site located in the hydrophobic interior of the membrane. In each of these instances, little is

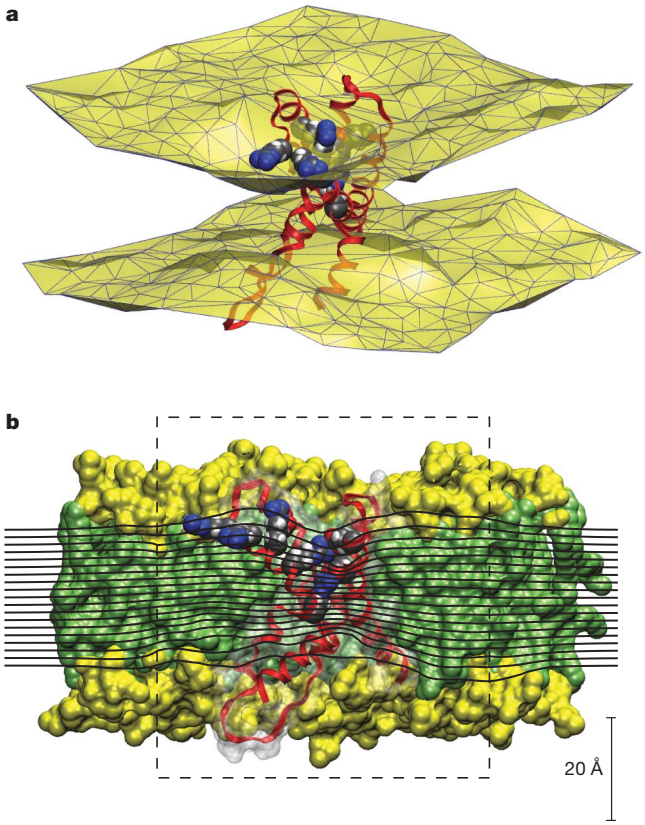

Figure 5 | Effects of the voltage-sensing domain on a lipid bilayer as revealed by molecular dynamics simulation. **a**, The lipid bilayer interface, represented as a two-dimensional Delaunay triangulation for the average positions of lipid carbonyl carbon atoms, reveals local distortions around the voltage-sensing domain. **b**, The transmembrane equipotential surfaces (black lines; contour interval is 5% of the applied potential) on a slice passing through the system centre (the Arg 133–Asp 62 salt bridge) show focusing features in the cavities of the voltage-sensing domain. Contributions to the molecular surface from aliphatic chains (green), polar groups (yellow), and proteins (white, transparent) of the corresponding cut-away view are shown as background. The dashed box indicates the region of the system considered atomistic in the calculation of the transmembrane potential (Methods). In both panels, the voltage-sensing domain is in ribbon representation (red) with the outer four Arg residues in S4, and their salt-bridge partners, shown in CPK representation and coloured by atom (carbon, grey; nitrogen, blue; oxygen, red; hydrogen, white).

known about the structure of the surrounding lipid membrane or whether adaptations may be important in the mechanism of the protein.

METHODS SUMMARY

The S1–S4 domain of K_vAP was expressed and purified as previously described[4] and reconstituted into a 1:1 mixture of POPC and POPG using rapid dilution of detergent micelles containing the protein and lipids. We prepared lipid multilayer samples for neutron diffraction by deposition of aqueous dispersions of liposomes on glass slides. A solution containing ~4 mg of lipid was applied to the glass surface (15-mm diameter), dried under vacuum and rehydrated using water vapour in a sealed chamber containing saturated salt solutions. Three types of sample were prepared, the first using a protonated voltage-sensing domain and protonated lipid, the second using a deuterated voltage-sensing domain and protonated lipid, and the third using a protonated voltage-sensing domain and head-group-deuterated POPC lipid (D4 lipid: $(CH_3)_3$-N-C^2H_2-C^2H_2-).

Oriented multilayers (~10-μm thick, corresponding to 2,000–3,000 bilayers) were transferred into the sample chamber of the neutron diffractometer and hydrated through the vapour phase at a temperature of 298 K. Neutron diffraction measurements were performed at the Advanced Neutron Diffractometer/Reflectometer[37], located at the US National Institute of Standards and Technology Center for Neutron Research, Maryland. Monochromatic cold neutrons of wavelength $\lambda = 5$ Å and a wavelength spread of $\Delta\lambda/\lambda = 1\%$ were diffracted by the sample and counted with a pencil-type ^{3}He detector. Specular $\Theta - 2\Theta$ scans were made to ensure that the momentum transfer (Q_z, typically 0–1.2 $Å^{-1}$) between the incident and diffracted neutron wavevectors was always perpendicular to the multilayer plane, thus probing the direction normal to the bilayer (Supplementary Fig. 1). We performed solid-state NMR experiments on proteoliposome pellets in ^1H_2O or ^2H_2O at a water/lipid ratio of 30:1. Lipid spectra were recorded on an 800-MHz Bruker AV800 spectrometer equipped with a 4-mm $^1H/^{13}C/^2H$ cross-polarization magic-angle-spinning probe (Bruker BioSpin). All-atom molecular dynamics simulations of the S1–S4 domain of K_vAP were carried out in POPC bilayers hydrated with, respectively, 9 and 11 water molecules per lipid (corresponding to experiments at relative humidities of 86% and 93%). Each system consisted of two stacked lipid bilayers, each containing a single S1–S4 domain, arranged to form a single pseudo-centrosymmetric unit cell. The simulations were run at a constant temperature of 295 K and a constant pressure of 1 bar.

Full Methods and any associated references are available in the online version of the paper at www.nature.com/nature.

Received 13 July; accepted 24 September 2009.

1. Swartz, K. J. Sensing voltage across lipid membranes. *Nature* **456,** 891–897 (2008).
2. Murata, Y., Iwasaki, H., Sasaki, M., Inaba, K. & Okamura, Y. Phosphoinositide phosphatase activity coupled to an intrinsic voltage sensor. *Nature* **435,** 1239–1243 (2005).
3. Lee, S. Y., Letts, J. A. & MacKinnon, R. Functional reconstitution of purified human Hv1 H+ channels. *J. Mol. Biol.* **387,** 1055–1060 (2009).
4. Jiang, Y. *et al.* X-ray structure of a voltage-dependent K^+ channel. *Nature* **423,** 33–41 (2003).
5. Long, S. B., Tao, X., Campbell, E. B. & MacKinnon, R. Atomic structure of a voltage-dependent K^+ channel in a lipid membrane-like environment. *Nature* **450,** 376–382 (2007).
6. Seoh, S. A., Sigg, D., Papazian, D. M. & Bezanilla, F. Voltage-sensing residues in the S2 and S4 segments of the Shaker K^+ channel. *Neuron* **16,** 1159–1167 (1996).
7. Aggarwal, S. K. & MacKinnon, R. Contribution of the S4 segment to gating charge in the Shaker K^+ channel. *Neuron* **16,** 1169–1177 (1996).
8. Jiang, Y., Ruta, V., Chen, J., Lee, A. & MacKinnon, R. The principle of gating charge movement in a voltage-dependent K^+ channel. *Nature* **423,** 42–48 (2003).
9. Cuello, L. G., Cortes, D. M. & Perozo, E. Molecular architecture of the KvAP voltage-dependent K^+ channel in a lipid bilayer. *Science* **306,** 491–495 (2004).
10. Ruta, V., Chen, J. & MacKinnon, R. Calibrated measurement of gating-charge arginine displacement in the KvAP voltage-dependent K^+ channel. *Cell* **123,** 463–475 (2005).
11. Alabi, A. A., Bahamonde, M. I., Jung, H. J., Kim, J. I. & Swartz, K. J. Portability of paddle motif function and pharmacology in voltage sensors. *Nature* **450,** 370–375 (2007).
12. Sands, Z. A. & Sansom, M. S. How does a voltage sensor interact with a lipid bilayer? Simulations of a potassium channel domain. *Structure* **15,** 235–244 (2007).
13. Chakrapani, S., Cuello, L. G., Cortes, D. M. & Perozo, E. Structural dynamics of an isolated voltage-sensor domain in a lipid bilayer. *Structure* **16,** 398–409 (2008).
14. Schmidt, D., Jiang, Q. X. & MacKinnon, R. Phospholipids and the origin of cationic gating charges in voltage sensors. *Nature* **444,** 775–779 (2006).
15. Ramu, Y., Xu, Y. & Lu, Z. Enzymatic activation of voltage-gated potassium channels. *Nature* **442,** 696–699 (2006).
16. Milescu, M. *et al.* Interaction between lipids and voltage sensor paddles detected with tarantula toxins. *Nature Struct. Mol. Biol.* **16,** 1080–1085 (2009).
17. Xu, Y., Ramu, Y. & Lu, Z. Removal of phospho-head groups of membrane lipids immobilizes voltage sensors of K^+ channels. *Nature* **451,** 826–829 (2008).
18. Asamoah, O. K., Wuskell, J. P., Loew, L. M. & Bezanilla, F. A fluorometric approach to local electric field measurements in a voltage-gated ion channel. *Neuron* **37,** 85–97 (2003).
19. Starace, D. M. & Bezanilla, F. A proton pore in a potassium channel voltage sensor reveals a focused electric field. *Nature* **427,** 548–553 (2004).
20. Chanda, B., Asamoah, O. K., Blunck, R., Roux, B. & Bezanilla, F. Gating charge displacement in voltage-gated ion channels involves limited transmembrane movement. *Nature* **436,** 852–856 (2005).
21. Ahern, C. A. & Horn, R. Focused electric field across the voltage sensor of potassium channels. *Neuron* **48,** 25–29 (2005).
22. Yang, N. & Horn, R. Evidence for voltage-dependent S4 movement in sodium channels. *Neuron* **15,** 213–218 (1995).
23. Larsson, H. P., Baker, O. S., Dhillon, D. S. & Isacoff, E. Y. Transmembrane movement of the shaker K^+ channel S4. *Neuron* **16,** 387–397 (1996).
24. Starace, D. M. & Bezanilla, F. Histidine scanning mutagenesis of basic residues of the S4 segment of the Shaker K^+ channel. *J. Gen. Physiol.* **117,** 469–490 (2001).
25. Neale, E. J., Rong, H., Cockcroft, C. J. & Sivaprasadarao, A. Mapping the membrane-aqueous border for the voltage-sensing domain of a potassium channel. *J. Biol. Chem.* **282,** 37597–37604 (2007).
26. Tombola, F., Pathak, M. M. & Isacoff, E. Y. Voltage-sensing arginines in a potassium channel permeate and occlude cation-selective pores. *Neuron* **45,** 379–388 (2005).
27. Freites, J. A., Tobias, D. J. & White, S. H. A voltage-sensor water pore. *Biophys. J.* **91,** L90–L92 (2006).
28. Jogini, V. & Roux, B. Dynamics of the Kv1.2 voltage-gated K^+ channel in a membrane environment. *Biophys. J.* **93,** 3070–3082 (2007).
29. Treptow, W. & Tarek, M. Environment of the gating charges in the Kv1.2 Shaker potassium channel. *Biophys. J.* **90,** L64–L66 (2006).
30. Worcester, D. L. & Franks, N. P. Structural analysis of hydrated egg lecithin and cholesterol bilayers. II. Neutrol diffraction. *J. Mol. Biol.* **100,** 359–378 (1976).
31. Blasie, J. K., Schoenborn, B. P. & Zaccai, G. Direct methods for the analysis of lamellar neutron diffraction from oriented multilayers: a difference Patterson deconvolution approach. *Brookhaven Symp. Biol.* **27,** 58–67 (1976).
32. Jacobs, R. E. & White, S. H. The nature of the hydrophobic binding of small peptides at the bilayer interface: implications for the insertion of transbilayer helices. *Biochemistry* **28,** 3421–3437 (1989).
33. Wiener, M. C. & White, S. H. Structure of a fluid dioleoylphosphatidylcholine bilayer determined by joint refinement of x-ray and neutron diffraction data. III. Complete structure. *Biophys. J.* **61,** 434–447 (1992).
34. Vamvouka, M., Cieslak, J., Van Eps, N., Hubbell, W. & Gross, A. The structure of the lipid-embedded potassium channel voltage sensor determined by double-electron-electron resonance spectroscopy. *Protein Sci.* **17,** 506–517 (2008).
35. Lee, A. G. Measurement of lipid-protein interactions in reconstituted membrane vesicles using fluorescence spectroscopy. *Methods Mol. Biol.* **27,** 101–107 (1994).
36. McIntosh, T. J. & Holloway, P. W. Determination of the depth of bromine atoms in bilayers formed from bromolipid probes. *Biochemistry* **26,** 1783–1788 (1987).
37. Dura, J. A. *et al.* AND/R: advanced neutron diffractometer/reflectometer for investigation of thin films and multilayers for the life sciences. *Rev. Sci. Instrum.* **77,** 074301 (2006).
38. Grossfield, A., Pitman, M. C., Feller, S. E., Soubias, O. & Gawrisch, K. Internal hydration increases during activation of the G-protein-coupled receptor rhodopsin. *J. Mol. Biol.* **381,** 478–486 (2008).
39. Ader, C. *et al.* Structural rearrangements of membrane proteins probed by water-edited solid-state NMR spectroscopy. *J. Am. Chem. Soc.* **131,** 170–176 (2009).
40. Lindahl, E. & Sansom, M. S. Membrane proteins: molecular dynamics simulations. *Curr. Opin. Struct. Biol.* **18,** 425–431 (2008).
41. Phillips, R., Ursell, T., Wiggins, P. & Sens, P. Emerging roles for lipids in shaping membrane-protein function. *Nature* **459,** 379–385 (2009).
42. Huang, H. W. Deformation free energy of bilayer membrane and its effect on gramicidin channel lifetime. *Biophys. J.* **50,** 1061–1070 (1986).
43. Nielsen, C., Goulian, M. & Andersen, O. S. Energetics of inclusion-induced bilayer deformations. *Biophys. J.* **74,** 1966–1983 (1998).
44. Goulian, M. *et al.* Gramicidin channel kinetics under tension. *Biophys. J.* **74,** 328–337 (1998).
45. Tabarean, I. V., Juranka, P. & Morris, C. E. Membrane stretch affects gating modes of a skeletal muscle sodium channel. *Biophys. J.* **77,** 758–774 (1999).
46. Laitko, U., Juranka, P. F. & Morris, C. E. Membrane stretch slows the concerted step prior to opening in a Kv channel. *J. Gen. Physiol.* **127,** 687–701 (2006).
47. Schmidt, D. & Mackinnon, R. Voltage-dependent K^+ channel gating and voltage sensor toxin sensitivity depend on the mechanical state of the lipid membrane. *Proc. Natl Acad. Sci. USA* **105,** 19276–19281 (2008).
48. Rosenbaum, D. M., Rasmussen, S. G. & Kobilka, B. K. The structure and function of G-protein-coupled receptors. *Nature* **459,** 356–363 (2009).
49. Krishnamurthy, H., Piscitelli, C. L. & Gouaux, E. Unlocking the molecular secrets of sodium-coupled transporters. *Nature* **459,** 347–355 (2009).
50. Erez, E., Fass, D. & Bibi, E. How intramembrane proteases bury hydrolytic reactions in the membrane. *Nature* **459,** 371–378 (2009).

Supplementary Information is linked to the online version of the paper at www.nature.com/nature.

Acknowledgements We thank the US National Institutes of Health (NIH) National Institute of Neurological Disorders and Stroke (NINDS) DNA sequencing facility for DNA sequencing, H. Jaffe in the NINDS protein sequencing facility for mass spectrometry and peptide sequencing and T. Kitaguchi for cloning K_vAP. We also thank T. Kimura, M. Mayer, M. Milescu, J. Mindell and S. Silberberg for discussions. This work was supported by the Intramural Research Programs of the NINDS, NIH (K.J.S.), and the National Institute on Alcohol Abuse and Alcoholism, NIH (K.G.); NIH grants GM74737 (S.H.W.) and Program Project GM86685 from the NINDS and the National Institute of General Medical Science (S.H.W., D.J.T.); and US National Science Foundation (NSF) grant CHE-0750175 (D.J.T.). We are grateful for allocation of computer time on the NSF-supported Teragrid resources provided by the Texas Advanced Computing Center, and the support of the National Institute of Standards and Technology, US Department of Commerce, in providing the neutron research facilities used for neutron diffraction experiments. The identification of any commercial product or trade name does not imply endorsement or recommendation by the US National Institute of Standards and Technology.

Author Contributions D.K. performed the biochemistry experiments; M.M., D.K. and D.L.W. performed the neutron diffraction experiments; D.K. and K.G. performed the solid-state NMR experiments; and J.A.F. and E.V.S. performed molecular dynamics simulations. All authors contributed to the study design and to writing the manuscript.

Author Information Reprints and permissions information is available at www.nature.com/reprints. Correspondence and requests for materials should be addressed to S.H.W. (stephen.white@uci.edu) or K.J.S. (swartzk@ninds.nih.gov).

METHODS

Voltage-sensing-domain expression, solubilization and purification. The K_vAP gene was amplified from *Aeropyrum pernix* genomic DNA using PCR and cloned into the pQE-60 vector (Qiagen). A pQE-60 plasmid containing the S1–S4 voltage-sensing domain of K_vAP (amino acid residues Met 1–Lys 147) was obtained by deletion of the carboxy-terminal region of K_vAP using PCR and its sequence was confirmed by DNA sequencing. The recombinant voltage-sensing domain was expressed in XL1-Blue strain of *Escherichia coli* as previously described[4]. The plasmid was transformed into the chemically competent *E. coli* cells (subcloning grade; Stratagene). One colony was inoculated into 100 ml LB broth supplemented with ampicillin ($100\,\mu g\,ml^{-1}$) and grown overnight at 37 °C with continuous shaking at 200 r.p.m. One litre of LB–ampicillin broth was inoculated with 10 ml of the starting culture and the protein expression was induced with 1 mM isopropyl-β-D-thiogalactopyranoside (Calbiochem) when the absorbance of the cells at 600 nm reached 0.6. After 3 h of induction, cells were harvested by centrifugation at 5,000*g* for 20 min.

Cells were resuspended in 10 mM EDTA solution and collected by centrifugation, and then twice resuspended in 20 mM Tris/HCl, 100 mM KCl, pH 7.8 and collected by centrifugation. Cells were then resuspended in 40 ml of 20 mM Tris/HCl, 100 mM KCl, pH 7.8 buffer, supplemented with 100 µl of protease inhibitor cocktail (Sigma) and 100 µl of $26\,mg\,ml^{-1}$ PMSF in isopropanol. Cells were sonicated for 5 min on ice, 50 µl of protease inhibitor cocktail was added, and the S1–S4 domain was extracted by solubilization of the homogenate in 2.5% (w/v) decylmaltoside (Anatrace) in 20 mM Tris/HCl, 100 mM KCl, pH 7.8. Lysate was then centrifuged at 100,000*g* for 1 h at 4 °C and the supernatant collected. Supernatant was mixed with Co-TALON resin (Clontech), the mixture was transferred to a chromatography column (Bio-Rad) and the solution was allowed to pass through. The resin with bound protein was washed with 0.25% (w/v) decylmaltoside, 10 mM imidazole in 20 mM Tris/HCl, 100 mM KCl, pH 7.8. Buffer was then exchanged for 3% (w/v) *n*-octyl-β-D-glucopyranoside (OG) in 20 mM Tris/HCl, 100 mM KCl, pH 7.8 and the protein eluted with 400 mM imidazole in the same buffer. One unit of thrombin (Sigma) was added per milligram of protein and the mixture was dialyzed against 3% (w/v) OG in 20 mM Tris/HCl, 100 mM KCl, pH 7.8 overnight at 4 °C in a dialysis cassette with a molecular-weight cut-off of 10 kDa (Pierce).

The protein was analysed by SDS–PAGE electrophoresis, followed by Coomassie staining (Invitrogen) and by MALDI-MS using the Invitrosol MALDI protein solubilizer kit (Invitrogen). The efficiency of the thrombin cleavage and the His-tag removal during the dialysis was confirmed using the His-Probe HRP reagent kit (Pierce) and by MALDI-MS. S1–S4 K_vAP protein identity was confirmed by mass spectrometric analysis of protein digest fragments and N-terminal Edman sequencing. Amino-terminal sequencing revealed that the first five amino acids are removed during protein expression, consistent with earlier observations[4]. The uniformly deuterated protein was obtained by expression in BioExpress media (Cambridge Isotope Laboratories) supplemented with 80% ^2H_2O, and the molecular weight of the purified protein was determined by MALDI-MS using the Invitrosol MALDI protein solubilizer kit (Invitrogen). The concentration of the protein was determined spectrophotometrically using an extinction coefficient ($\varepsilon_{280\,nm} = 17{,}210\,M^{-1}\,cm^{-1}$) calculated from the deduced protein composition[51].

Lipid reconstitution of the voltage-sensing domain of K_vAP. The S1–S4 voltage-sensing domain of K_vAP were reconstituted to different molar ratios of protein and lipid as previously described[14,52–54], using a 1:1 mixture of POPC and POPG. All lipids were purchased from Avanti Polar Lipids and mixtures were dried from solution in chloroform under a stream of nitrogen gas and desiccated under vacuum overnight. Lipid films were solubilized in 20 mM Tris/HCl, 100 mM KCl buffer, pH 7.8 with 3% (w/v) OG, and protein was added to the lipid to form mixed detergent–lipid micelles. Proteoliposomes were formed by rapid dilution of the mixed protein–detergent–lipid micelles well below the critical micelle concentration of the OG detergent. Proteoliposome pellets were collected by ultracentrifugation at 200,000*g* at 4 °C using an Optima TL 100 TLX ultracentrifuge and 100.3 TLA rotor (Beckman). Proteoliposome pellets were resuspended in H_2O and sedimented by ultracentrifugation, resuspended and mildly sonicated for 1 min in a water-bath sonicator. The resultant proteoliposomes were analysed for lipid content using the method of ref. 55, and residual detergent contents were determined using the modified phenol-sulphuric acid assay[56] and by dissolving aliquots of the sample in deuterated MeOH and analysis of the components of the mixture by ^1H NMR.

Circular dichroism spectroscopy. Circular dichroism spectra were recorded in 20 mM Tris/HCl, 100 mM KCl buffer, pH 7.8, using a JASCO J-815 spectropolarimeter equipped with a thermally controlled cuvette holder. Spectra were recorded on voltage-sensing-domain samples in 0.1–1-mm quartz cuvettes, from 180 nm to 250 nm with 1-nm step resolution and 4-s integration time. The helix content of the protein sample was calculated following ref. 57, and indicated that the protein had high (~85%) helical content both in OG micelles and when reconstituted in lipid, consistent with the X-ray structure of the S1–S4 domain of K_vAP[4] and EPR results on the S1–S4 domain and full-length K_vAP channel[9,13].

Fluorescence spectroscopy. Fluorescence emission spectra for Trp 70 within the S2 helix of the voltage-sensing domain of K_vAP were recorded for the protein in either OG micelles or when reconstituted into lipid. (Trp 70 is the only Trp residue within S1–S4.) Fluorescence spectra were recorded in 20 mM Tris/Cl, 100 mM KCl, pH 7.4 at 25 °C with stirring in a total volume of 2 ml using the SPEX FluoroMax 3 spectrofluorometer. Quartz 1 cm × 1 cm cuvettes were used for all fluorescence measurements. An excitation wavelength of 295 nm (5-nm band pass) was used and the emission was scanned between 300 and 400 nm (5-nm band pass) with an increment of 0.5 nm. The polarizer was configured to excitation-90°, emission-0° (ref. 58) and emission spectra of OG buffer or lipid alone were subtracted. Quenching of Trp 70 fluorescence was examined by titration with acrylamide, an aqueous quencher of Trp fluorescence. Stern–Volmer quenching constants, K_{SV}, were calculated from the best fits of $F_0/F = 1 + K_{SV}[Q]$, where F_0 and F are the fluorescences of the Trp 70 in the absence and presence of a quencher, respectively, and $[Q]$ is the concentration of the quencher. To determine the disposition of the Trp 70 in model membranes, we compared quenching by bromine atoms attached to different positions on the hydrocarbon tail[35,36,59]. For these experiments, protein was reconstituted into proteoliposomes using a 1:1 mixture of POPG and either Br_2(6,7)-PC (1-palmitoyl-2-stearoyl(6-7)dibromo-*sn*-glycero-3-phosphatidylcholine, C16:0, C18:0), Br_2(9,10)-PC (1-palmitoyl-2-stearoyl(9-10)dibromo-*sn*-glycero-3-phosphatidylcholine, C16:0, C18:0) or Br_2(11,12)-PC (1-palmitoyl-2-stearoyl(11-12)dibromo-*sn*-glycero-3-phosphatidylcholine, C16:0, C18:0).

Determining structure from neutron diffraction data and deuterium contrast variation. Lamellar diffraction patterns yield trans-bilayer distributions of scattering length projected onto the bilayer normal (z axis), which we call bilayer profiles and write as $\rho(z)$. The profiles presented here have been placed on the absolute per-lipid scale. The simplest profiles are obtained by Fourier transformation of the measured structure factors $F_M(h) = \sqrt{I_h}$, where I_h is the corrected intensity of the hth diffracted intensity. In this case, $\rho(z)$ varies along the bilayer normal and has an average value of zero when integrated over the unit cell defined by the Bragg spacing, d. The amplitude of $\rho(z)$ is arbitrary, determined only by the units used to measure intensities, such as neutron counts observed in a given time period. This simple approach provides limited information about the disposition of molecules dissolved within the bilayer.

Useful information can be obtained only when the profiles are placed on an absolute scale, meaning that the average value of $\rho(z)$, ρ_0, corresponds to the total scattering length of the unit cell and that the variation of $\rho(z)$ around ρ_0 shows absolute changes in scattering-length density. To determine ρ_0, the contents of the unit cell (lipid, water and protein) must be known. To calibrate the variation of $\rho(z)$, an isomorphous substitution of atoms of known scattering length, b_{sub}, must be introduced into the sample. In this case, the integral over the unit cell of the 'difference profile', $\Delta\rho(z) \equiv \rho_{sub}(z) - \rho(z)$, must equal b_{sub}. This procedure, described in detail in refs 32, 60, 61, yields instrumental constants, $k(h)$, that lead to absolute-scale structure factors, $F(h) = k(h)F_M(h)$. For a centrosymmetric bilayer containing two lipids per unit cell, the average scattering-length density is given by $\rho_0 = (2/Sd)\sum b_i$, where S is the area per lipid and $\sum b_i$ is the sum of the scattering lengths of all of the atoms in the unit cell. The value of S is rarely known. To circumvent this problem, we can use the 'relative absolute scale'[32], in which $\rho^*(z) = S\rho(z)$. A better and more descriptive term is the per-lipid scale, because the scattering-length density describes the scattering length per lipid rather than per unit volume. To use this scale, we need to know only the average numbers per lipid of water molecules and other components in the unit cell. As stated, the profiles here have been placed on the absolute per-lipid scale.

The absolute per-lipid scattering-length density is given by

$$\rho*(z) = \rho*_0 + \frac{2}{d}\sum_{h=1}^{h_{max}} \varphi(h)|F(h)| \cos\left(\frac{2\pi hz}{d}\right) \quad (1)$$

where $\varphi(h)$ is the sign of the absolute-scale structure factor, $F(h)$ (whose absolute value is $|F(h)|$), and h_{max} indexes the highest observable structure factor. The unit cell is centrosymmetric; consequently, in the data presented here $\varphi(h) = \pm 1$ (that is, $\cos(0)$ or $\cos(\pi)$). Methods for determining the signs have been discussed in detail elsewhere[30,31].

Treatment of diffraction data. In the kinematical approximation, the structure factors, $F(h)$, at all observed diffraction orders are determined as the square root of the integrated peak intensities, after background correction, absorption correction (B) and Lorentz-factor correction ($\sin(2\theta_h)$), where θ_h denotes the angle

of incidence corresponding to the hth order of diffraction. The absorption correction was calculated as follows, where t is the sample thickness and α is the linear absorption coefficient[30]: $B(h) = \sin(\theta_h)/(2\alpha t)[1 - \exp(-2\alpha t/\sin(\theta_h))]$. We determined phases by measuring a sample in a series of different ^1H_2O–^2H_2O contrasts (that is, using different mole fractions of ^2H_2O in the salt solutions for hydrating the sample). Assuming a Gaussian distribution of water hydrating the lipid head groups[60], the difference structure factors corresponding to a lipid bilayer hydrated with ^2H_2O (F_D) and, respectively, ^1H_2O (F_H) can be modelled according to

$$\Delta F(h) = k_D F_D(h) - k_H F_H(h) = x_D \exp[-(\pi h A/d)^2] \cos(2\pi h Z/d) \qquad (2)$$

where A and Z respectively denote the 1/e half-width and the mean position of the Gaussian describing the labelled component distribution (water in this case), and k_D and k_H are scale factors. The prefactor x_D scales with the amount of deuterium per lipid: $x_D = 2(b_D - b_H)f_D n_D$, where b_H and b_D are the scattering lengths of deuterium and hydrogen, respectively, f_D is the fraction of deuterated component and n_D is the number of deuterium atoms per molecule in the labelled component. The cosine factor in equation (2) determines the slope of the linear dependence, $\Delta F(h) = f(x_D)$, and thus the phases $\varphi(h)$.

To determine the trans-bilayer distributions of water, the -CH_2-CH_2- group of the phosphorylcholine (PC), and the S1–S4 domain of K_vAP, we substituted those molecular components for their deuterated counterparts, for both protein-containing or pure-lipid samples, and compared their density profiles with those of protonated samples using the absolute per-lipid scale.

Scaling of the neutron data and determination of the amount of water per lipid. Because the raw diffraction intensities collected are not normalized, the absolute (per-lipid) scale is determined on the basis of the sample composition (for example protein concentration and amount of water). The protein concentration was determined from ultraviolet absorbance at 280 nm, but the amount of water accumulated in the protein-containing membranes at the relative humidity of our experiments is unknown and has to be determined by additional experiments. We used a lipid-deuteration scheme (manuscript in preparation) that includes deuteration of the water of hydration (^2H_2O) and the PC-C^2H_2-C^2H_2- group (D4 lipid) to resolve the absolute scale and the number of waters per lipid. The two homologous samples (protonated and D4 lipid) were each measured under at least two different ^1H_2O–^2H_2O contrast conditions by exchanging ^1H_2O with ^2H_2O in different proportions (for example ^1H_2O/^2H_2O ratios of 100:0, 50:50 and 80:20) in the saturated salt solutions used in the chamber. Both the water and the D4 lipid are components that can be described by Gaussian distributions[33,60]. In equation (2), we compare the data from the protonated- and D4-lipid homologous samples, measured in either ^1H_2O or 20% ^2H_2O, to determine the parameters describing the D4-lipid distribution. Knowing the prefactor x_D, we determine the position Z and width A, as well as the scale factors k_H (protonated lipid) and k_D (D4 lipid), by a least-squares minimization procedure. Once scaled, the data collected in ^1H_2O and 20% ^2H_2O for a given sample are compared in equation (2) to determine the water distribution parameters and the number of water molecules per lipid, represented by the prefactor x_D in equation (2). The water content of neat-POPC multilayers determined using this approach is indistinguishable from that determined by independent methods[62].

Molecular dynamics simulations. Two simulation systems with 9 and 11 water molecules per lipid, respectively, and 130 lipid molecules per protein (corresponding to relative humidities of 86% and 93% and a protein/lipid molar ratio of 0.77 mol%) were prepared from the end configuration of a simulation trajectory of the S1–S4 domain of K_vAP in a POPC bilayer with excess water[27]. The initial atomistic model in the excess-water simulation corresponded to residues 24 to 147 in the model of the K_vAP full channel proposed in ref. 63. The pore domain of the full-channel model provides an unambiguous constraint for the orientation of the S1–S4 domain in the lipid bilayer. The final placement of the protein in the lipid bilayer along the transmembrane direction was determined by ensuring that the five Tyr side chains in the S2–S3 connecting turn and the S3–S4 end were simultaneously in contact with the head-group region on opposite sides of the lipid bilayer. Further details of the set-up of the excess-water simulation system and the generation of molecular dynamics trajectories can be found in ref. 27.

The low-hydration simulation systems consisted of two stacked lipid bilayers, each containing a single S1–S4 domain, arranged to form a single pseudo-centrosymmetric unit cell. The system with nine water molecules per lipid was prepared by removing the necessary water and lipid molecules from the end configuration of the excess-water simulation. The initial equilibration consisted of 1,000 steps of energy minimization followed by a 1-ns molecular dynamics run at constant volume and constant temperature (295 K), with the protein backbone held fixed. The full simulation was then carried out at a constant temperature of 295 K and a constant pressure of 1 atm. The protein was progressively released from its initial configuration over the first 5.5 ns using harmonic restraints. The simulation was carried out in the absence of restraints for 37.5 ns. The system with 11 water molecules per lipid was prepared from the end configuration of the system with nine water molecules per lipid by adding the necessary number of water molecules. The initial equilibration consisted of 1,000 steps of energy minimization followed by a 20-ps run at constant volume and constant temperature (295 K) over the newly added waters, and an 80-ps run over the whole system. The full simulation was then carried out at a constant temperature of 295 K and a constant pressure of 1 atm for 25.2 ns.

All of the molecular dynamics trajectories were generated with the NAMD 2.6 software package[64]. The CHARMM22 and the revised CHARMM27 force fields[65–67] were used for the peptide and the lipids, respectively, and the TIP3P model was used for water[68]. The smooth particle mesh Ewald (PME) method[69,70] was used to calculate electrostatic interactions, and the short-range real-space interactions were cut off at 11 Å, using a switching function. A reversible multiple-time-step algorithm[71] was used to integrate the equations of motion with time steps of 4 fs for electrostatic forces, 2fs for short-range non-bonded forces and 1 fs for bonded forces. All bond lengths involving hydrogen atoms were held fixed using the SHAKE and SETTLE algorithms. A Langevin dynamics scheme was used for thermostatting. Nose–Hoover–Langevin pistons were used for pressure control[72,73]. Molecular graphics and simulation analyses were performed with the VMD 1.8.6 software package[74] over the last 10 ns of each simulation.

To compare simulations with 11 water molecules per lipid directly with the experimental data, neutron diffraction structure factors[75] for the nth order of diffraction, $F(n)$, were computed from the molecular dynamics trajectory according to

$$F(n) = \sum_j^{\text{cell}} b_j \exp(2\pi i n z_j/d) \qquad (4)$$

where the sum is over all the atoms in the simulation unit cell; b_j and z_j are the neutron scattering length and z coordinate of the jth atom, respectively; the Bragg spacing, d, is taken to be half of the simulation cell length along the transmembrane direction; and n is an integer. The scaling factor of half the simulation cell length for the spatial coordinates corresponds to the repeat distance (Bragg spacing) of an oriented stack of bilayers. The oriented bilayers diffract as centrosymmetric objects independent of the presence of the protein. The purpose of the double-bilayer simulation system is to model the two equally probable orientations of the protein in the lipid bilayer. Therefore, because the total scattering length of a single simulation cell is twice that of a single repeat unit in the diffraction experiment, each atom in the simulation cell is considered to have an occupation factor of one-half. Structure factors were averaged over ten system configurations (one per nanosecond of trajectory time), and the total scattering-density profiles were constructed from the structure factors exactly as in the analysis of the experimental diffraction data (see equation (1)). Component densities were computed following the experimental protocol (see equation (2)), assuming uniform labelling at the same mole fraction as in the neutron diffraction experiments. The average length of the simulation cell in the dimension perpendicular to the membranes was 104 Å, corresponding to a spacing of $d = 51.8$ Å for a single bilayer containing the S1–S4 voltage-sensing domain of K_vAP, in excellent agreement with the experimental value of 52 Å obtained at 93% relative humidity (corresponding to 11 water molecules per lipid).

The electrostatic potential in the excess-hydration simulation was calculated using the linearized Poisson–Boltzmann theory, treating all the system components as linear, isotropic dielectrics under an applied potential difference across the membrane, as previously described[76–78]. For a given configuration along the simulation trajectory, the electrostatic potential was calculated over a composite system consisting of a cuboid region of space (dashed rectangle in Fig. 5b) containing the atomistic configurations of the protein and most of the lipids. This region was considered to be embedded in a continuum composed of a semi-infinite planar slab, representing the membrane, between two half-spaces that represent the electrolyte solution[77]. The calculations were performed over the last 16 ns of the simulation trajectory, taking one configuration per nanosecond, using the PBEQ module of the CHARMM 32a2 software package[79]. The linearized Poisson–Boltzmann equation was solved by finite differences, using the successive over-relaxation method, over a cubic grid of 161 nodes with a grid spacing of 1 Å. The continuum slab thickness was set to equal the separation between carbonyl distributions in the atomistic system. A dielectric constant of two was assigned to lipids and protein. The solvent dielectric constant was set to 80 and the salt concentration was set to 150 mM. The molecular surface was used to define the atomistic dielectric boundaries using the van der Waals radii from the CHARMM force field[65].

NMR saturation transfer difference using magic-angle spinning. Saturation transfer difference experiments[80] were used to study hydration of the voltage-sensing domains in membranes. Magic-angle-spinning (MAS) conditions were

used as previously described[38,81] to resolve lipid resonances. ^{1}H NMR spectra of lipids were recorded and resonance attenuation measured in response to radio-frequency pulses. The saturating radio-frequency pulses (field strength, $(\gamma/2\pi)B_1 = 0$–1.2 kHz) consisted of twenty Gaussian-shaped 50-ms pulses. The saturation frequency was set to the amide region of the protein (8.5 p.p.m.) or the water resonance (4.79 p.p.m.). The attenuation of the lipid methylene signal, defined as resonance amplitude recorded without saturation divided by the amplitude recorded with saturation, was followed as indicator of magnetization transfer to lipid. The proteoliposomes were packed into 4-mm MAS rotors (Bruker) and hydrated with either ^2H_2O or ^1H_2O to the final water/lipid ratio of 30:1. Sixteen scans with a recycle delay of 10 s were acquired at 295.1 K. All spectra were recorded on an 800-MHz Bruker AV800 spectrometer equipped with a 4-mm ^{1}H/^{13}C/^{2}H CP-MAS probe (Bruker BioSpin) at a MAS frequency of 10 kHz.

51. Gill, S. C. & von Hippel, P. H. Calculation of protein extinction coefficients from amino acid sequence data. *Anal. Biochem.* **182,** 319–326 (1989).
52. Heginbotham, L., Kolmakova-Partensky, L. & Miller, C. Functional reconstitution of a prokaryotic K^+ channel. *J. Gen. Physiol.* **111,** 741–749 (1998).
53. Perozo, E., Cortes, D. M. & Cuello, L. G. Three-dimensional architecture and gating mechanism of a K^+ channel studied by EPR spectroscopy. *Nature Struct. Biol.* **5,** 459–469 (1998).
54. Cuello, L. G., Romero, J. G., Cortes, D. M. & Perozo, E. pH-dependent gating in the *Streptomyces lividans* K^+ channel. *Biochemistry* **37,** 3229–3236 (1998).
55. Hurst, R. O. The determination of nucleotide phosphorus with a stannous chloride-hydrazine sulphate reagent. *Can. J. Biochem. Physiol.* **42,** 287–292 (1964).
56. Dubois, M., Gilles, K., Hamilton, J. K., Rebers, P. A. & Smith, F. A colorimetric method for the determination of sugars. *Nature* **168,** 167 (1951).
57. Chen, Y. H., Yang, J. T. & Chau, K. H. Determination of the helix and beta form of proteins in aqueous solution by circular dichroism. *Biochemistry* **13,** 3350–3359 (1974).
58. Ladokhin, A. S., Jayasinghe, S. & White, S. H. How to measure and analyze tryptophan fluorescence in membranes properly, and why bother? *Anal. Biochem.* **285,** 235–245 (2000).
59. Abrams, F. S. & London, E. Extension of the parallax analysis of membrane penetration depth to the polar region of model membranes: use of fluorescence quenching by a spin-label attached to the phospholipid polar headgroup. *Biochemistry* **32,** 10826–10831 (1993).
60. Wiener, M. C., King, G. I. & White, S. H. Structure of a fluid dioleoylphosphatidylcholine bilayer determined by joint refinement of X-ray and neutron diffraction data. I. Scaling of neutron data and the distributions of double bonds and water. *Biophys. J.* **60,** 568–576 (1991).
61. Wiener, M. C. & White, S. H. Transbilayer distribution of bromine in fluid bilayers containing a specifically brominated analogue of dioleoylphosphatidylcholine. *Biochemistry* **30,** 6997–7008 (1991).
62. Hristova, K. & White, S. H. Determination of the hydrocarbon core structure of fluid dioleoylphosphocholine (DOPC) bilayers by X-ray diffraction using specific bromination of the double-bonds: effect of hydration. *Biophys. J.* **74,** 2419–2433 (1998).
63. Lee, S. Y., Lee, A., Chen, J. & MacKinnon, R. Structure of the KvAP voltage-dependent K^+ channel and its dependence on the lipid membrane. *Proc. Natl Acad. Sci. USA* **102,** 15441–15446 (2005).
64. Phillips, J. C. *et al.* Scalable molecular dynamics with NAMD. *J. Comput. Chem.* **26,** 1781–1802 (2005).
65. MacKerell, A. D. Jr *et al.* All-atom empirical potential for molecular modeling and dynamics studies of proteins. *J. Phys. Chem. B* **102,** 3586–3616 (1998).
66. Feller, S. E. & MacKerell, A. D. Jr. An improved empirical potential energy function for molecular simulations of phospholipids. *J. Phys. Chem. B* **104,** 7510–7515 (2000).
67. Klauda, J. B., Brooks, B. R., MacKerell, A. D. Jr, Venable, R. M. & Pastor, R. W. An ab initio study on the torsional surface of alkanes and its effect on molecular simulations of alkanes and a DPPC bilayer. *J. Phys. Chem. B* **109,** 5300–5311 (2005).
68. Jorgensen, W. L., Chandrasekhar, J., Madura, J. D., Impey, R. W. & Klein, M. L. Comparison of simple potential functions for simulating liquid water. *J. Chem. Phys.* **79,** 926–935 (1983).
69. Darden, T., York, D. & Pedersen, L. Particle mesh Ewald: an *N*.log(*N*) method for Ewald sums in large systems. *J. Chem. Phys.* **98,** 10089–10092 (1993).
70. Essmann, U. *et al.* A smooth particle mesh Ewald method. *J. Chem. Phys.* **103,** 8577–8593 (1995).
71. Grubmüller, H., Heller, H., Windemuth, A. & Schulten, K. Generalized Verlet algorithm for efficient molecular dynamics simulations with long-range interactions. *Mol. Simul.* **6,** 121–142 (1991).
72. Martyna, G. J., Tobias, D. J. & Klein, M. L. Constant-pressure molecular-dynamics algorithms. *J. Chem. Phys.* **101,** 4177–4189 (1994).
73. Feller, S. E., Zhang, Y., Pastor, R. W. & Brooks, B. R. Constant pressure molecular dynamics simulation: the Langevin piston method. *J. Chem. Phys.* **103,** 4613–4621 (1995).
74. Humphrey, W., Dalke, W. & Schulten, K. VMD: visual molecular dynamics. *J. Mol. Graph.* **14,** 33–38 (1996).
75. Benz, R. W., Castro-Román, F., Tobias, D. J. & White, S. H. Experimental validation of molecular dynamics simulations of lipid bilayers: a new approach. *Biophys. J.* **88,** 805–817 (2005).
76. Roux, B. Influence of the membrane potential on the free energy of an intrinsic protein. *Biophys. J.* **73,** 2980–2989 (1997).
77. Roux, B. The membrane potential and its representation by a constant electric field in computer simulations. *Biophys. J.* **95,** 4205–4216 (2008).
78. Grabe, M., Lecar, H., Jan, Y. N. & Jan, L. Y. A quantitative assessment of models for voltage-dependent gating of ion channels. *Proc. Natl Acad. Sci. USA* **101,** 17640–17645 (2004).
79. Brooks, B. R. *et al.* CHARMM: the biomolecular simulation program. *J. Comput. Chem.* **30,** 1545–1614 (2009).
80. Forsen, S. H. A. Study of moderately rapid chemical exchange reactions by means of nuclear magnetic double resonance. *J. Chem. Phys.* **39,** 2892–2901 (1963).
81. Soubias, O. & Gawrisch, K. Probing specific lipid-protein interaction by saturation transfer difference NMR spectroscopy. *J. Am. Chem. Soc.* **127,** 13110–13111 (2005).